Chemistry–A European Journal
Research Article
doi.org/10.1002/chem.202403095
Chemistry Europe
European Chemical Societies Publishing
www.chemeurj.org

Role of Secondary Structure and Time-Dependent Binding on Disruption of Phthalocyanine Aggregates by Guanine-Rich Nucleic Acids

Eleanor R. Windle,[a] Christopher C. Rennie,[b] Robert M. Edkins,*[b] and Susan J. Quinn*[a]

Phthalocyanines are versatile photodynamic therapy agents whose biological activity depends on their aggregation state, which is expected to be influenced by binding to biomolecules. Here, guanine-rich nucleic acid binding of a water-soluble cationic, regiopure C_{4h} zinc phthalocyanine bearing four triethylene glycol methyl ether and four *N*-methyl-4-pyridinium substituents (**1**) is reported. In contrast to double-stranded DNA, guanine systems **GpG**, **$(GG)_{10}$**, **poly(G)** and **quadruplex DNA** are shown to effectively disrupt phthalocyanine aggregates in buffered solution. This process is accompanied by evolution of the Q-band absorbance and enhanced emission. Increasing the sequence length from **GpG** to **$(GG)_{10}$** increases the binding and confirms the importance of multiple binding interactions. Enhanced binding in the presence of KCl suggests the importance of nucleobase hydrogen-bonded mosaics in phthalocyanine binding. Notably, the **$(GT)_{10}$** sequence is even more effective than quadruplex and pure guanine systems at disrupting the aggregates of **1**. Significant time-dependent binding of **1** with **poly(G)** reveals biexponential binding over minutes and hours, which is linked to local conformations of **poly(G)** that accommodate monomers of **1** over time. The study highlights the ability of biomacromolecules to disrupt phthalocyanines aggregates over time, which is an important consideration when rationalizing photoactivity of photosensitizers in-vivo.

Introduction

Phthalocyanines (Pcs) possess strong far-red to near-infrared (NIR) light absorption and can act as effective phototherapy,[1,2] photoacoustic,[3] and fluorescence imaging agents.[4] In particular, the ability of Pcs to harness NIR photons expands their phototherapy application to tissues deeper than the skin while reducing photosensitivity for patients.[5] The therapeutic efficacy is further enhanced by their potential to act as agents for photodynamic therapy (PDT) through singlet-oxygen photosensitization or photothermal therapy (PTT) through effective heat generation, with potential to combine these effects.[5] So far, five Pcs have reached clinical testing for PDT (Photosens, photocycanine, Pc4, CGP55847, and IR700DX)[2] and many others have been reported in recent years.[6] Furthermore, Pcs have been investigated in combination with other anti-cancer agents to improve therapeutic outcomes.[7]

Significant effort has been directed to the development of Pcs with optimized PTT and PDT activity.[8] The PDT and PTT photoactivity of a Pc is typically governed by its aggregation state present at the biological target site.[8] Monomeric Pcs may undergo efficient intersystem crossing (ISC) allowing them to act as efficient PDT agents through either Type I (transfer of an electron or proton to form reactive oxygen species) or Type II (energy transfer to $^3O_2$ to form singlet oxygen ($^1O_2$)) mechanisms. On the other hand, aggregation of Pcs can enhance non-radiative decay facilitating local heating for PTT applications (Figure 1). As the hydrophobic nature of Pcs typically causes them to aggregate in aqueous buffered solution,[9] efforts have been made to reduce stacking by functionalizing the aromatic core with groups that increase steric hindrance and improve solubility.[10] The PDT activity of Si(IV) Pcs is in part attributed to the role of axial substituents in preventing aggregation.[11] An example of this was the incorporation of two axial oleate ligands to limit aggregation by introducing steric hindrance.[11b] Furthermore, Pcs have been shown to bind with high affinity to guanine-rich G-quadruplex DNA through favorable end-on π-stacking of the extended aromatic system with the G-quartet.[12] The presence of positively charged side chains has also been shown to lead to favorable interactions with quadruplex loops.[12a] Early reports demonstrated that Pc binding could cause inhibition of telomerase,[13] and reduce *NRAS* expression in cancer cells by selective photocleavage of the target RNA G-quadruplex.[14] These observations have led to significant interest in the study and application of G-quadruplex binding Pcs.[14–15] Exciting recent reports include the catalytic light

[a] E. R. Windle, Prof. S. J. Quinn
School of Chemistry
University College Dublin
Belfield, Dublin, Ireland
E-mail: susan.quinn@ucd.ie
[b] Dr. C. C. Rennie, Dr. R. M. Edkins
Department of Pure and Applied Chemistry
University of Strathclyde
Glasgow, Scotland, UK
E-mail: robert.edkins@strath.ac.uk

Supporting information for this article is available on the WWW under https://doi.org/10.1002/chem.202403095

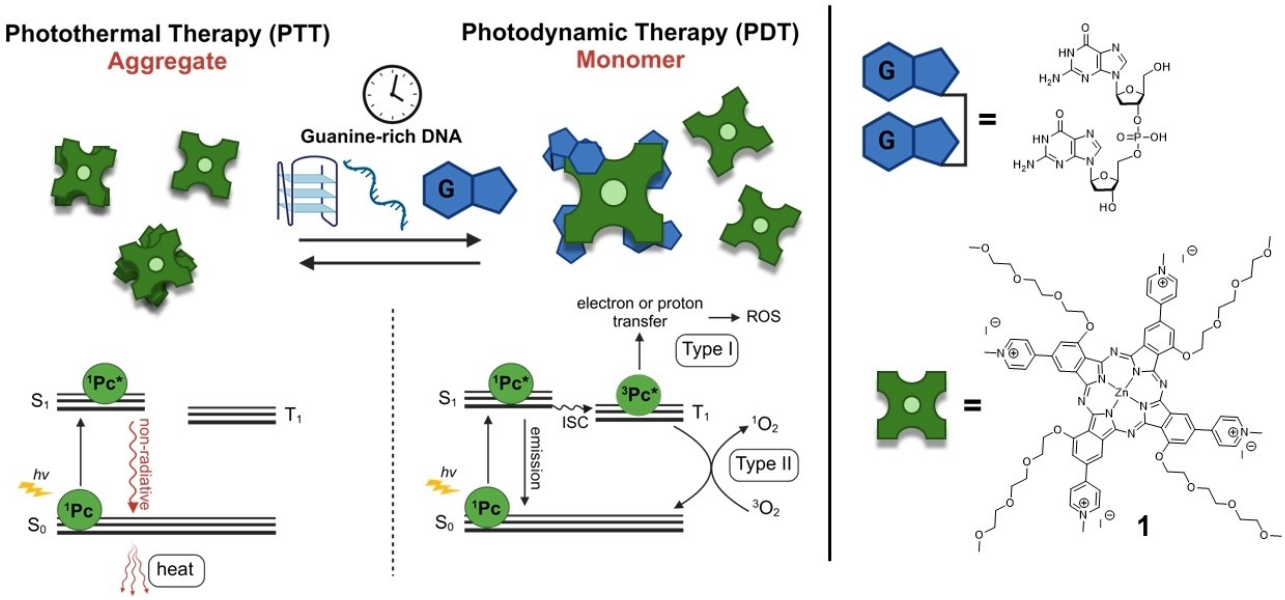

Figure 1. Systems under study. Simplified Jablonski diagram of photothermal and photodynamic therapy mechanisms and their link to phthalocyanine aggregation state and interactions with G-rich DNA (aggregate structure and DNA interaction shown are schematic). Structure of C_{4h} Pc **1** with four triethylene glycol methyl ether (TEG) groups in the α positions and four *N*-methyl-4-pyridinium groups in the β positions.

triggered photodegradation of G-quadruplex DNA by a Zn(II) Pc[12c] and the development of a zinc Pc-bound quadruplex system for combined PDT and antisense therapy.[16]

Charge is known to modulate the binding of Pcs to DNA and is also a key factor in cellular interactions and localization.[17] Interestingly, while cationic porphyrins such as TMPyP4 typically exhibit low selectivity for G-quadruplex over double stranded DNA (**dsDNA**), anionic Pcs have been shown to preferentially bind the G-quadruplex.[13a] These preferential interactions are attributed to removing the non-specific electrostatic interactions associated with the cationic species.[18] Despite their lower binding affinity, anionic Pcs have shown to inhibit telomerase,[13a] decrease NRAS expression[14] and been successfully used for photodynamic cancer therapy.[19] In addition to showing stronger binding affinity, cationic Pcs have been found to show greater photoactivity in cells, which is attributed to the influence of environmental pH, interaction with bio-membranes and binding to serum proteins, leading to differences in subcellular localization.[17] Preparation of amido Pcs with different methylene units separating the Pc core from peripheral ammonium groups has been used to modulate the aggregation and DNA binding.[20] We are interested in developing light-activated systems to target quadruplex DNA and have previously studied the interaction of cationic transition metal polypyridyl complexes to different quadruplex DNA systems.[21]

Typically, Pc monomers are required to access the longer-lived triplet excited states needed for PDT, while PTT effects are linked to thermal deactivation of aggregates. However, there have also been reports of the PDT activity of aggregates.[8] Additionally, Pcs formulated as aggregates have been shown to dissociate and release monomers to the target site where they are detected in the monomer form by the appearance of fluorescence.[22] The possibility of dual PDT and PTT mechanisms, and the switching between them, has often not been considered. The disruption of the aggregates may arise due to interactions with a range of biomolecules at the cell surface, with the cell membrane, or with intracellular molecules. As noted above, Pcs have been shown to impact cellular function by targeting nucleic acids. Therefore, it is of interest to explore the ability of different nucleic acid structures to disrupt Pc aggregates and to consider the timescale over which the phenomenon occurs. This is particularly relevant in the case of polymer DNA, which can take time to achieve optimum binding. Time-dependent binding of DNA has previously been observed for threading binuclear polypyridine ruthenium intercalators, where fast initial surface binding to polymeric DNA is followed by a slow intercalation process that occurs over hours.[23] As Pc aggregates are expected to range from small clusters to larger assemblies and nano-sized aggregates it is also relevant to note the ability of nucleic acids to overcome the collective van der Waals interactions in aggregates of nanocarbons. We previously showed that natural **dsDNA** disperses aggregates of single-walled carbon nanotubes (SWNTs) over multiple days.[24]

In this current study we explore the ability of guanine-rich nucleic acid sequences to disrupt aggregates of a cationic zinc

Pc containing four triethylene glycol methyl ether (TEG) solubilizing groups in the α positions and four *N*-methyl-4-pyridinium solubilizing groups in the β positions (Figure 1). We show that increasing sequence length from the guanine deoxyribonucleotide monophosphate (**dGMP**) to the deoxy dinucleotide (**GpG**) and 20-mer guanine deoxy oligonucleotide $(\mathbf{GG})_{10}$, results in improved disruption of aggregates of **1** leading to monomer species. Furthermore, our results show that G-quadruplexes and sequences capable of forming hydrogen bonding mosaics are effective at dispersing monomer forms of **1**. Finally, we show that in all cases additional time-dependent binding plays a role in the disruption of aggregates of **1**.

Results and Discussion

Synthesis of Cationic TEG Zinc Phthalocyanine (1)

Two challenges associated with exploiting Pcs for PDT are poor solubility and the use of mixtures of regioisomers for certain substituted derivatives. Kobayashi[25] reported previously that hydrophilic and biocompatible triethylene glycol methyl ether (TEG) groups in the 3-position of a phthalonitrile precursor can direct, through both steric and electronic effects, the regioselective synthesis of the C_{4h} H_2Pc derivative with four TEG groups in the α positions of the resultant Pc. While this derivative is more water compatible than unsubstituted Pcs, it still requires an organic cosolvent such as DMSO to dissolve fully and is therefore not suitable as a photosensitizer. Building on Kobayashi's work, we recently reported a strategy to introduce secondary functionality in four of the β positions while maintaining the C_{4h} regioselective Pc synthesis.[26] Using this strategy, one of our previously reported derivatives had four additional 4-pyridyl groups (compound **TEGPyrPc**). Here, we sought to use this compound as a starting point to make a water-soluble Pc suitable for DNA-binding studies through methylation of the 4-pyridyl groups, which should also increase DNA binding through Coulombic interactions. We first metalated the Pc using $Zn(OAc)_2 \cdot 2H_2O$ in *N*,*N*-dimethylformamide (DMF) to give Zn derivative **ZnTEGPyrPc** in 73% yield (Scheme 1). Methylation of the pyridyl groups of **ZnTEGPyrPc** initially proved troublesome; reaction with dimethyl sulfate did not fully methylate all four pyridyl groups, while use of MeOTf promptly led to decomposition, as observed by a loss of green color. However, heating **ZnTEGPyrPc** with a large excess of iodomethane in DMF at 80 °C in a sealed vessel led to the desired tetramethylated compound **ZnTEGQPyrPc**, subsequently referred to as **1**, as a tetraiodide salt in 97% yield. ^{1}H NMR analysis of **1** and mass spectrometry (Figure S1–S3) confirmed the complete methylation of the four pyridyl units of **1**, while the ^{1}H NMR spectrum further supported the regioselective synthesis through its well-resolved *J*-coupling patterns (Figure S2). **1** can be dissolved in pure water without a cosolvent.

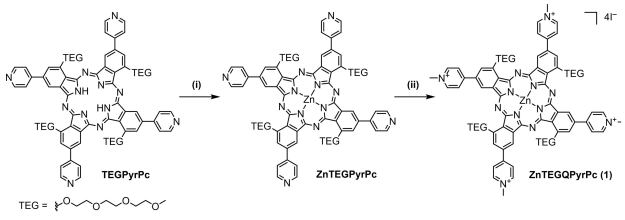

Scheme 1. Synthesis of compound **1** (**ZnTEGQPyrPc**) from **TEGPyrPc**. (i) $Zn(OAc)_2 \cdot 2H_2O$ (20 eq.), DMF, 120 °C, 24 h, 73%. (ii) MeI, DMF, 80 °C, 24 h, 97%.

Spectroscopic Characterization of 1

In DMSO solution, the monomeric form of **1** is observed and characterized by Soret absorption between 380 nm and 500 nm and the strongly absorbing, well-resolved and sharp Q_{00} band in the NIR region at 737 nm with an extinction coefficient of 1.74×10^5 M^{-1} cm^{-1} accompanied by a weaker Q_{01} band at 662 nm (Figure 2). In DMSO solution, a linear increase in absorption with increasing concentration is observed between 0.28 and 6.5 μM (Figure S4), further evidencing monomeric behavior in DMSO over this concentration range.

In water, the Soret band absorption of **1** at 416 nm is reduced and most notably, the Q-band has a significantly lower absorbance with a blue shift from 739 nm to 730 nm (167 cm^{-1}) and an additional band is present at 686 nm, while at the red edge the Q-band extends further to 855 nm. These spectral changes are evidence of Pc stacking and aggregation[27] and can be related to previous studies of zinc Pc derivatives in water/DMSO mixtures that have shown the formation of higher aggregates with increased %v/v water. π-Stacking with a twisting about the intermolecular Zn–Zn axis can lead to a H-/J-type transition with such new absorption spectral features either side of the monomeric Q band maximum.[28] The impact of the increased addition of water to a DMSO solution of **1** is shown in Figure S5.

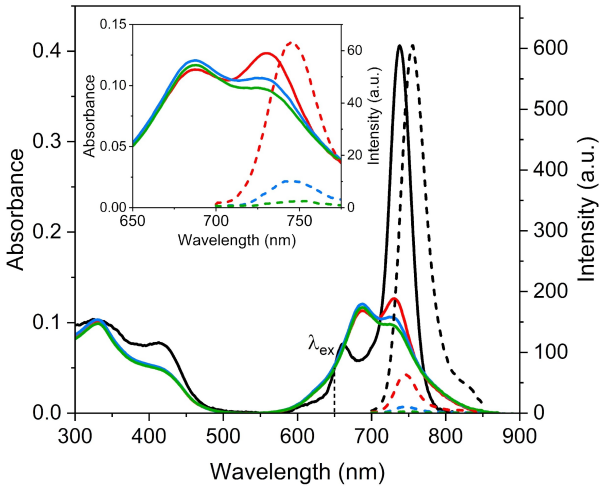

Figure 2. Absorption (solid) and emission (λ_{ex} = 650 nm) (dash) spectra of **1** (2.3 μM) in DMSO (black), water (red), 10 mM potassium phosphate buffer (blue), and 50 mM potassium phosphate buffer + 100 mM KCl (green) at 25 °C. Inset shows an expansion of the Q-band region for the absorption and emission spectra of the aqueous solutions.

The presence of aggregates of **1** in solution was also confirmed by dynamic light scattering (DLS) measurements, which show greater changes to the autocorrelation function with increasing water content, see Figure S6A. Such changes have previously been used to identify the formation of molecular aggregates in solution.[29] When **1** is dispersed in 100% water a clear decay is observed indicating the presence of aggregates and this signal is found to decrease at 50% water and disappear under conditions where monomers are expected to be present. These DLS measurements are found to be in close agreement with the visible absorption and emission behavior of **1** in the monomer and mixed state, see Figure S6B–C. Further changes to the absorbance spectrum are observed in 10 mM potassium phosphate buffer solution, with a decrease in Q-band absorbance by 17% and a blue-shift of the Q-band to 726 nm. A further 8% decrease in Q-band absorbance was observed when the buffer concentration was increased to 50 mM with 100 mM KCl, see Figure 2. In both water and buffer solution a linear increase in absorbance is observed for concentrations between 0.2 and 25 μM (Figure S7–S8). In DMSO solution, strong monomer emission at 755 nm is observed (Φ_f = 0.12). The emission intensity decreased by 89% in water and by a further 84% in 10 mM phosphate buffer and again by 76% in 50 mM phosphate buffer with 100 mM KCl due to the dominance of non-radiative decay in aqueous solutions caused by the aggregation.[27] In addition, the emission is shifted to 746 nm in water and 745 nm in buffer solution. An excitation spectrum confirmed that it is the residual monomer in solution that is responsible for emission in water, as seen by the close resemblance to the DMSO solution absorption spectrum rather than to that in water (Figure S9). Addition of 1% pyridine to an aqueous solution of **1** also gave rise to an absorption spectrum that resembled that of the monomeric form recorded in DMSO, as axial coordination to the Zn disrupts the aggregates. These measurements show that, despite its tetracationic nature, **1** strongly aggregates in aqueous solution. This is more pronounced in a buffered environment, which is likely due to some screening of any modest electrostatic repulsion observed in water. Overall, the population of aggregated **1** is found to be very sensitive to the solution environment.

Binding Interactions with G-Rich Nucleic Acids

Next the binding interactions of **1** with different nucleic acid systems (Figure S10) was investigated. First the ability of mononucleotide (**dGMP**), dinucleotide (**GpG**) and 20-mer **$(GG)_{10}$** guanine DNA to form monomers of **1** by disrupting aggregates formed in buffered solutions was explored. To do this, increasing concentrations of the guanine systems were added to **1** (2.3 μM) in 10 mM potassium phosphate buffered solution. In the absence of DNA, **1** is weakly emissive and the absorption spectrum of **1** shows a band at 686 nm and a Q-band at 726 nm characteristic of the aggregated state. Increasing additions of **dGMP** of up to 120 nucleobase:**1** (Nucl:Pc) stoichiometric equivalents caused a decrease in the Pc absorbance and emission, which was attributed to additional aggregation or loss of **1** from solution (Figure S11). A similar effect was also observed upon the addition of buffer solution (Figure S12). In contrast, the addition of **GpG** at the same nucleobase equivalent resulted in a dramatic change in the absorption spectrum (Figure 3A). The Q-band absorbance was found to increase, accompanied by a bathochromic shift of 16 nm to 742 nm (297 cm^{-1}), and a decrease in the Soret band absorption at 416 nm was observed, which is characteristic of DNA binding.[30] The weak emission detected in 10 mM buffer solution was enhanced by a 17-fold increase in emission intensity at 753 nm which indicates an increase of monomeric **1** in solution, see Figure 3B. The disruption of aggregates of **1** was even more pronounced upon addition of **$(GG)_{10}$** (Figure S13C–D), which was found to be effective at disaggregating **1** at half the nucleobase equivalent (Nucl:Pc = 60) of the dinucleotide (Figure 3E). These results show the ability of short sequences of DNA to disrupt aggregated **1** and the contrast in behavior of **dGMP** and **GpG** suggests the importance of multiple binding interactions.

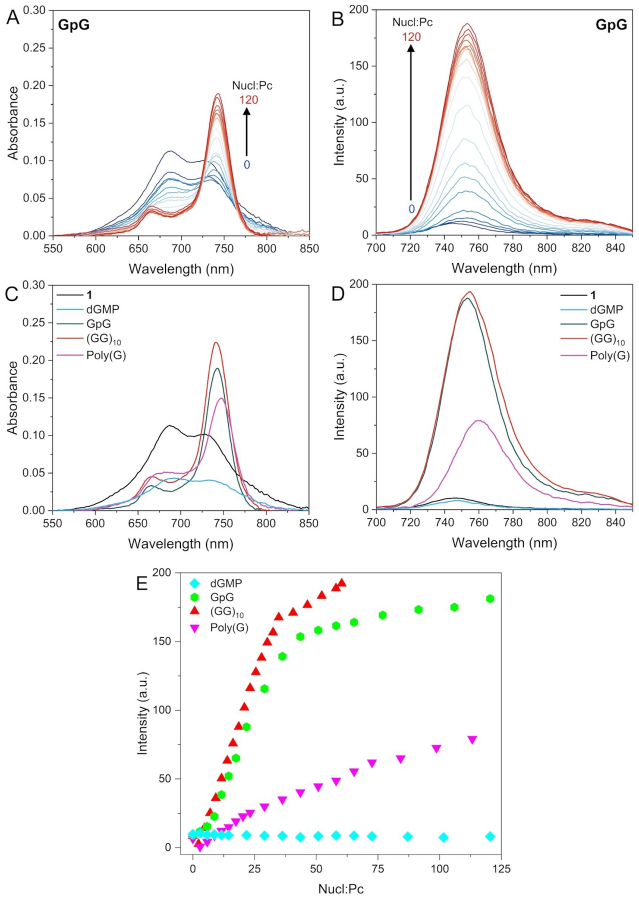

Figure 3. (A) Absorption and (B) emission spectra (λ_{ex} = 650 nm) of **1** (2.3 μM) titrated against increasing concentration of **GpG** (0–259 μM Nucleobase). (C) Absorption and (D) emission spectra of **1** at start and end of titration with G-rich nucleic acids with [Nucl]:[Pc] = 120 (**dGMP**, **GpG**), 60 (**$(GG)_{10}$**), and 113 (**poly(G)**) (E) Emission intensity of **1** in the presence of nucleic acids against [Nucl]:[Pc]. All spectra in 10 mM potassium phosphate buffer at 25 °C.

Next, we considered the ability of the polyguanylic ribonucleic acid (**poly(G)**) to disrupt aggregates of **1**, which was chosen as it is a readily available polymeric form of guanine. The addition of large stoichiometric equivalents (Nucl:Pc = 113) of **poly(G)** resulted in modest changes to the absorption and emission spectra, see Figure S13E–F and Figure 3C–D. This may be due to the ability of the polynucleotide to adopt locally folded motifs that inhibit binding to the aggregates of **1**. The ability of the four guanine systems to disrupt aggregates of **1** formed in 10 mM potassium phosphate buffer is given in Figure 3E. Overall titration results of the G-rich nucleic acid systems highlights the inability of **dGMP** to disrupt aggregates and the need for significantly greater nucleobase equivalents of **poly(G)** compared to **GpG** and $(GG)_{10}$ to disrupt the same quantity of aggregates of **1**.

Binding to Quadruplex and Double-Stranded DNA

The binding of **1** to the hybrid G-quadruplex formed from the human telomere sequence (**G-HT**)[31] and anti-parallel G-quadruplex formed by the *Oxytricha* telomere ($G_4T_4G_4$)[32] repeat oligonucleotide in the presence of 100 mM KCl was examined. In both structures the non-guanine bases lie in the loops of the quadruplex flanking the G-tetrad core.[15a] The addition of **G-HT** was accompanied by the appearance of strong Q-band absorption and a 67-fold increase in the emission (Figure 4A–B). A bathochromic shift of 18 nm was observed for the Q-band and the plateau of absorbance was approached upon the addition of ca. two quadruplex equivalents, see Figure 4E. Similar changes were also observed for $G_4T_4G_4$, with a slightly greater bathochromic shift in the Q-band absorption (21 nm) observed. These results demonstrate that **1** can bind readily to quadruplex-forming DNA resulting in a shift from aggregate to DNA-bound monomer species in solution. Of the G-rich sequences, $(GT)_{10}$ was found to be the most effective at disrupting aggregates of **1** (Figure 4E). The addition of relatively low stoichiometric equivalents resulted in the greatest change in the Q-band absorbance (2.6-fold increase upon 30 Nucl:Pc addition).

In contrast to what is observed in the presence of quadruplex DNA, only a small enhancement in the luminescence of **1** was observed in the presence of double-stranded DNA formed from either the mixed base self-complementary sequence $(dGCGCATATGCGC)_2$ (**DDD-AT**), which is related to the Dickerson–Drew DNA sequence,[33] or natural polymeric DNA **dsDNA**. In both cases negligible luminescent enhancement was observed in 50 mM potassium phosphate buffer with 100 mM KCl, (Figure 4E), while slightly greater enhancement is observed in the absence of salt in 10 mM buffer conditions (Figure S15A–B and S17A–B). This trend of modest/negligible enhancement was also observed in the presence of single stranded natural DNA (**ssDNA**), see Figure 4E and S17E–H.

Guanine bases are known to self-assemble in solution and G-rich DNA can form quadruplex structures in the presence of stabilizing cations.[34] When the binding to the G-rich sequences was repeated under the conditions of 100 mM KCl, the changes to the Q-band absorbance and the emission enhancement were found to increase (Table S3). The impact was found to be

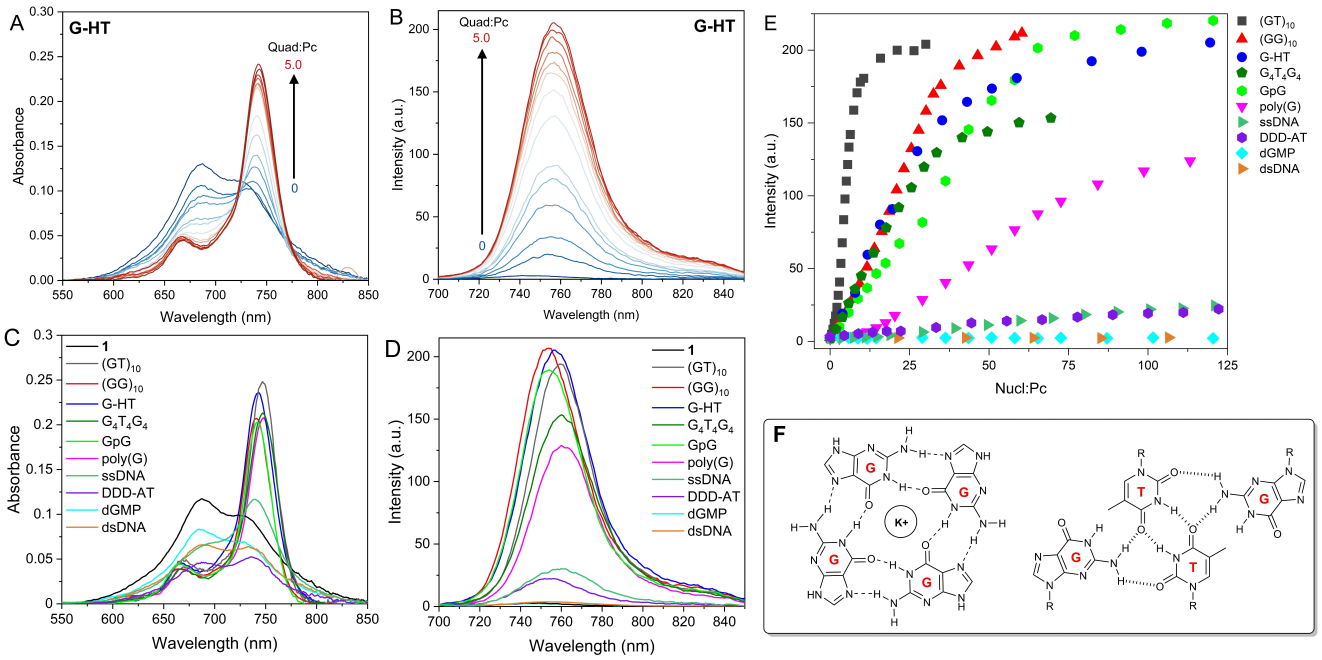

Figure 4. (A) Absorption and (B) emission spectra (λ_{ex} = 650 nm) of **1** (2.3 μM) titrated against increasing concentration of **G-HT** (0 - 10.8 μM Quadruplex). (C) Absorption and (D) emission spectra of **1** at start and end of titration with nucleic acids with [Nucl]:[Pc] = 30 ($(GT)_{10}$), 60 ($(GG)_{10}$), 120 (**G-HT**, **GpG**, **DDD-AT**, **dGMP**), 70 ($G_4T_4G_4$), 113 (**poly(G)**), 130 (**ssDNA**), and 380 (**dsDNA**). (E) Emission intensity of **1** in the presence of nucleic acids against [Nucl]:[Pc]. (F) Schematic of G-tetrad and GT-mosaic. All spectra in 50 mM potassium phosphate buffer with 100 mM KCl at 25 °C.

greatest for **poly(G)**, where a 1.5-fold increase in Q-band absorbance was observed in the absence of KCl compared to a 2-fold increase in the presence of 100 mM KCl. A summary of the results of the nucleic acid titration studies in the presence of KCl is given in Table 1. The comparative studies performed in the absence and presence of 100 mM KCl indicate that the presence of a G-tetrad template (Figure 4F) may facilitate the binding of Pcs and the disruption of aggregates. Furthermore, **$(GG)_{10}$** was found to be more effective than **poly(G)** at disrupting the aggregates of **1** (Figure 4E). This may indicate more effective guanine quartet formation in the shorter oligonucleotide than in the **poly(G)**. The importance of guanine quartet formation is further supported by the results of the binding between **1** and **poly(A)**, which show that **poly(A)** disperses **1** much less than **poly(G)**, see Figure S18. Though the purine footprint of adenine is similar to guanine, a key difference is that **poly(A)** participates in fewer intramolecular interactions compared to **poly(G)**.

Circular dichroism (CD) titrations were performed to gain further insight into the binding interactions that contribute to the Pc disaggregation and luminescent enhancement. In addition to providing structural information about nucleic acids, CD is very sensitive to structural changes that occur upon small molecule binding.[13b,20,35] This is particularly the case for guanine-rich sequences, which can adopt diverse secondary structures including a wide range of quadruplex structures.[36] The CD titrations revealed remarkable changes in the secondary structure of **G-HT**. Notably, a decrease in the ellipticity at 287 nm and increase at 267 nm in the CD spectrum was observed upon addition of increasing concentrations of **1** at room temperature (Figure 5). These changes are known to correspond to a transition from a hybrid to a parallel conformation.[13b,15b,36a,20] The observation of the transition at room temperature suggests that **1** possesses chaperone capabilities unlike other reported Pcs.[13b]

The UV–visible spectrum shows significant suppression of the Soret band as well as a significant bathochromic shift of the Q-band with 40% hypochromism compared to the spectrum of the monomer in DMSO, see Figure S19. Together these results suggest a preference for end-on stacking to the parallel structure. This may also explain the effective binding of **$(GG)_{10}$** whose CD spectrum shows a strong positive signal at 262 nm and a negative signal at 241 nm, which are characteristic of the presence of parallel quadruplex structures.

In contrast, no change was observed in the CD spectrum upon addition of **1** to the **$G_4T_4G_4$** anti-parallel quadruplex structure (Figure S20), which indicates that the addition of **1** does not alter the structure. This may be due to the greater barrier to structural transition for this quadruplex[37] and suggests that the Pc binds less well to the antiparallel structure. In the case of **poly(G)** the addition of increasing concentrations of **1** caused a decrease in the CD signal at 260 nm (Figure S21). This effect was observed to be greater in the presence of 100 mM KCl in 50 mM buffer than in the 10 mM buffer alone, which strongly suggests Pc-dependent partial disruption of local guanine stacking interactions.[35] Notably, a significant change in the CD signal of **$(GT)_{10}$** was observed with an inversion of ellipticity at 280 nm to a strong negative band at 266 nm and a positive band at 244 nm (Figure S22), which indicates that binding to **1** results in a dramatic change in the secondary structure of this nucleic acid. A positive band at *ca.* 305 nm was also observed to appear for **$(GT)_{10}$**. As DNA does not absorb in this region it may indicate some aggregation or possibly induced chirality of **1** in the presence of this nucleic acid sequence. As noted in the introduction, DNA has been shown to compete with favorable SWNT van der Waals interactions leading to dispersion of carbon nanomaterial aggregates.[24,38] The study of DNA/SWNT dispersions point to the importance of the formation of a mosaic structure through interbase hydrogen bonds as an explanation for the ability of guanine- and thymine-containing family of oligonucleotides $(GT)_n$ to disperse SWNTs (Figure 4F).[39] It is interesting to consider that the effectiveness of **$(GT)_{10}$** to disperse **1** may be related to its ability to form a hydrogen-bonded motif at the Pc hydrophobic face. Minimal changes to the CD spectra of **ssDNA**,

Table 1. Summary of the spectroscopic changes observed for 2.3 μM **1** in the presence of the different DNA systems in 50 mM potassium phosphate buffer and 100 mM KCl at 25 °C.

DNA	Nucl : Pc	ΔAbs[a]/Δnm[b]	I_f[c]	I/I_o[d]	λ_{em}[e]
$(GT)_{10}$	30	2.6/21 nm	204	68	759
$(GG)_{10}$	60	2.1/18 nm	212	66	753
G-HT	120	2.1/18 nm	205	67	757
$G_4T_4G_4$	70	2.1/21 nm	153	55	760
GpG	120	2.2/16 nm	224	70	753
Poly(G)	113	2.0/21 nm	124	41	761
ssDNA	130	1.2/14 nm	30	10	760
DDD-AT	120	0.5/9 nm	22	7.1	754
dsDNA	380	0.6/7 nm	4	1.6	754

[a] Absorbance at Q-band expressed in terms of the absorbance in the absence of DNA. absence of DNA. [b] Change in the Q-band wavelength from 726 nm in buffered solution. [c] Emission intensity following titration (λ_{ex} = 650 nm, arbitrary units). [d] Emission intensity (arbitrary units) following titration expressed in terms of emission in the absence of DNA (745 nm). [e] Wavelength of maximum emission intensity in the presence of DNA.

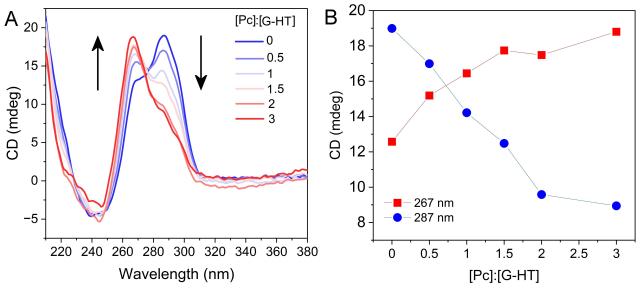

Figure 5. (A) Circular dichroism spectra of **G-HT** (3.2 μM quadruplex) titrated with **1** (0–9.5 μM) in 50 mM potassium phosphate buffer with 100 mM KCl at 25 °C. (B) Titration curve representing ellipticity at 267 nm and 287 nm against concentration ratio of **1** to **G-HT**.

DDD-AT and **dsDNA** were observed in the presence of **1** (Figure S23), which taken with the negligible binding that is observed in higher salt concentrations, suggests that the enhancement of luminescence observed in Figure 4E likely arises due to a small amount of electrostatic interaction in contrast to the effect of stacking interactions observed with G-rich sequences.

Time-Dependent Disaggregation and Kinetic Studies

AFM studies have shown that the secondary structure of **poly(G)** evolves from single-strand to quadruplex structures over time.[40] During a titration of **1** with **poly(G)** in the absence of KCl, the absorbance of the Q-band was observed to increase with time, which was accompanied by an increase in the emission. These observations indicated the role of time-dependent binding of **poly(G)** to **1**. To explore this further, the titration was repeated, and the end-point absorbance and emission measurements were recorded again after 24 h. A dramatic change in the absorbance spectrum was observed with a 70% increase in the Q-band absorbance, and the emission was found to double in intensity (Figure 6A–B). However, only modest changes were observed over 24 h in the presence of KCl (Figure 6A–B). As noted previously, **poly(G)** binding was found to improve in the presence of KCl, which was attributed to the cation-templated formation of G-tetrads. It is therefore likely that, in the absence of KCl, time is needed for the single-stranded regions to achieve optimum binding to disrupt the aggregates of **1**. Similar time-dependent interactions have been observed for the binding of natural DNA to SWNTs.[24]

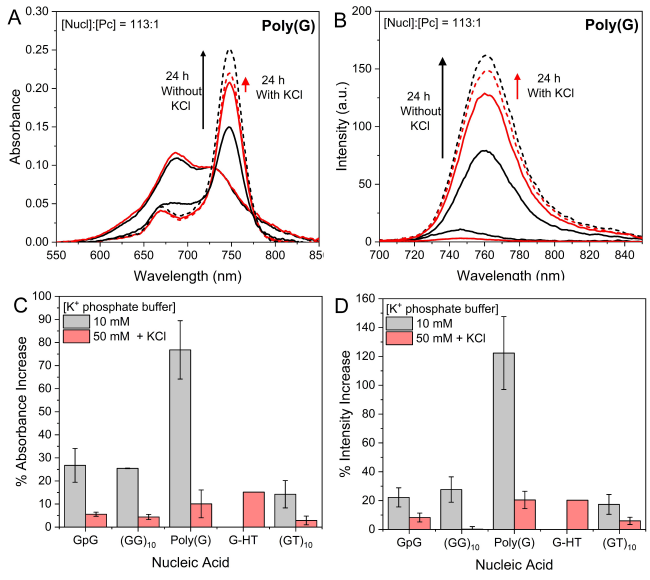

Figure 6. (A) Absorption and (B) emission spectra for **1** (2.3 μM) with **poly(G)** (0–245 μM) in 10 mM potassium phosphate buffer (black) and 50 mM potassium phosphate buffer + 100 mM KCl (red) and spectra after 24 h (dash). Percentage increase in (C) absorbance of Q-band (~747 nm) and (D) emission intensity 24 h after titration in 10 mM potassium phosphate buffer (grey) and 50 mM potassium phosphate buffer + 100 mM KCl (red) with different nucleic acids. All measurements performed at 25 °C.

An overview of the changes in the Q-band absorbance of **1** observed for the different nucleic acid systems after 24 is shown in Figure 6C. In the absence of KCl, between 15 and 25% increases in absorbance are observed, which are also reflected in the emission increases shown in Figure 6D. As was the case for **poly(G)**, less change was observed for the DNA oligos in the presence of KCl. For $(GG)_{10}$, at higher buffer strength there was no increase in the emission intensity 24 h following the titration compared to a 28% increase in 10 mM phosphate buffer (Figure 6D). However, the **G-HT** quadruplex was found to show a 15% increase in Q-band absorbance in this higher buffer strength, which was comparable to **poly(G)** under these conditions (Figure 6C–D). Note, very minimal changes occurred to the low luminescence enhancement of **ssDNA**, **DDD-AT**, and **dsDNA** after 24 h, see Figure S26–S28.

A kinetic study of the binding of **1** to **poly(G)** in the absence of KCl was performed by examining the influence of the (Nucl:Pc) stoichiometric ratio on the evolution of the Q-band absorbance with time. Figure 7A shows the Q-band absorbance of **1** recorded after 48 h incubation with between 10 and 120 guanine nucleobase equivalents of **poly(G)**. Figure 7B compares the Q-band absorbance recorded during the titration (circles) with that recorded 48 h later (squares), expressed as a percentage of the monomer absorbance of the same concen-

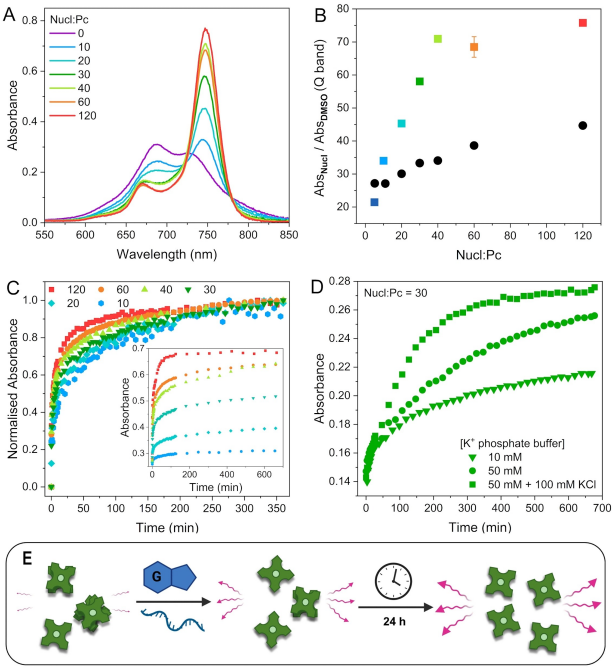

Figure 7. Time-dependent study of binding of **1** to **poly(G)**. (A) Absorption spectra for **1** (5.9 μM) 48 h after addition of **poly(G)** (0–658 μM, Nucl:Pc, 0–120) in 10 mM potassium phosphate buffer. (B) Absorbance at 747 nm expressed as a percentage of the absorbance of **1** (5.9 μM) in DMSO, showing extent of monomer liberated during the titration at equivalent Nucl:Pc ratio (black circles) compared to the timed experiment endpoints (squares). (C) Normalized absorbance at 747 nm in timed experiments. Inset shows absorbance at 747 nm up to 720 minutes. (D) Absorbance at 747 nm of **1** (2.3 μM) over 700 min with **poly(G)** (71 μM) in different buffer conditions. (E) Schematic of time-dependent changes to aggregation state of **1** and emission upon addition of nucleic acids. All measurements performed at 25 °C.

tration of **1** recorded in DMSO. This reveals that during the titration a Q-band absorbance of between 25 and 45% of the monomer absorbance in DMSO is observed at the different Nucl:Pc ratios. Importantly, Figure 7B shows a significant increase in Q-band absorbance across all guanine ratios when incubated for 48 h. Notably, for Nucl:Pc = 120 the Q-band absorbance is approx. 80% that of the monomer in solution, compared to approx. 45% DMSO equivalent monomer absorbance in the titration.

To further probe this phenomenon, the Q-band absorbance was monitored at 25 °C over 12 h, see inset Figure 7C. To highlight the changes, the normalized absorbance change recorded over 6 h is shown in Figure 7C, which shows a greater rate of binding at higher concentrations of **poly(G)**. Kinetic analysis reveals a bi-exponential process with initial changes occurring over minutes followed by a slower second process occurring over hours (Figure S29, Table 2). The data shows that both processes become faster with increasing Nucl:Pc. In the case of Nucl:Pc = 120, these processes occur with a rate constant of 1.5×10^{-1} min^{-1} (k_1) and 1.2×10^{-2} min^{-1} (k_2) extracted from the change in absorbance. Importantly, Figure 7D reveals that time-dependent interactions persist in a higher strength buffer and in 100 mM KCl. As the conditions approach that of physiological ionic strength, the rate of the increase in Q-band absorbance is found to increase. The origin of the time-dependent binding is likely attributed to the ability of the polymer to adopt different local intramolecular folding structures, which is common for biological macromolecules. It also may be related to the role of G-tetrad formation to achieve optimum binding.

Finally, the time-dependent interactions for $(GG)_{10}$, $(GT)_{10}$ and **poly(G)** at a Nucl:Pc of 30 were repeated in 10 mM phosphate buffer at physiological temperature (37 °C). While temperature is expected to impact the monomer–aggregate ratio, the visible absorption spectra confirms that **1** is in a predominantly aggregated form under physiological conditions. Notably, the extent and the rate of the disruption of aggregates was found to increase under these conditions, see Figures S30–S31. The kinetic analysis showed that a bi-exponential process persisted and in the case in **poly(G)** an increase in both rate constants was observed, while for $(GG)_{10}$ and $(GT)_{10}$ the faster process became more dominant, see Figure S32 and Table S4.

Table 2. Summary of time-dependent study of the absorption changes of **1** binding to **poly(G)** over 6 h in 10 mM potassium phosphate buffer at 25 °C. Rate constants k_1 and k_2 obtained by fitting to biexponential function.

[Nucl]:[Pc]	k_1 (min^{-1})	k_2 (min^{-1})
10	$1.3\pm0.3\times10^{-1}$ (33%)	$9.3\pm0.9\times10^{-3}$ (67%)
20	$3.4\pm0.4\times10^{-1}$ (42%)	$8.9\pm0.6\times10^{-3}$ (58%)
30	$2.0\pm0.1\times10^{-1}$ (46%)	$8.1\pm0.5\times10^{-3}$ (54%)
40	$1.9\pm0.1\times10^{-1}$ (48%)	$9.5\pm0.7\times10^{-3}$ (52%)
60	$1.5\pm0.1\times10^{-1}$ (55%)	$8.6\pm0.6\times10^{-3}$ (45%)
120	$1.5\pm0.1\times10^{-1}$ (63%)	$1.2\pm0.1\times10^{-2}$ (37%)

Conclusions

In this study, we investigated the ability of different DNA systems to disrupt the aggregation of a water-soluble cationic Pc (**1**) in aqueous buffered solution. We found that G-rich systems are very effective at dispersing aggregates of **1** while there was a notable lack of binding to **dsDNA** systems. The ability of guanine sequences to disperse **1** was found to increase with the oligo length from **dGMP** to $(GG)_{10}$. CD titrations revealed the ability of **1** to induce structural change in guanine-rich sequences and notably in the case of the **G-HT** quadruplex, to cause a transition from the hybrid form to the parallel structure. Similar to previously reported Pc binding studies, we observed effective binding of **1** to quadruplex structures, which further supports the role of templating nucleobase H-bonding in the stabilization. The importance of the formation of hydrogen-bonding mosaics or tetrad plates is supported by the limited capacity of **poly(A)** to disrupt aggregates of **1**.

Recently, the need for detailed studies of the aggregation state of Pcs in the biological environment when considering their PDT activity was raised.[8] A key observation of this present study was the role of time-dependent binding interactions. Cell studies typically consider the time-component in terms of uptake, but our time-dependent studies point to the evolution of aggregates to monomers in the presence of biological macromolecules. Overall, we observed that the ability of DNA to disrupt aggregates of **1** is linked to the DNA sequence and secondary structure. It is also intriguing to note that the most effective oligonucleotide at disrupting aggregates of **1** was the $(GT)_{10}$ 20-mer. Interestingly, the dinucleotide repetitive sequence, $(GT)_n$, is highly prevalent in eukaryotic genomes.[41] Taken together, these findings have implications for the mechanism of cellular activity of Pc photosensitizers in phototherapy, as they indicate that binding to biomacromolecules has the potential to pivot activity from a photothermal to photodynamic mechanism.

Acknowledgements

Financial support from the Research Ireland (GOIPG/2022/1362) for E. R. W. and from the University of Strathclyde for C. C. R. and for 'Global Engagements Funding' is acknowledged. Figure 1 and Figure 7E were created with Biorender.com. Open Access funding provided by IReL.

Conflict of Interests

The authors declare no conflict of interest.

Data Availability Statement

The data that support the findings of this study are available from the corresponding author upon reasonable request.

Keywords: phthalocyanines · DNA · time-dependent · disaggregation · guanine-rich

[1] a) M. Mitsunaga, M. Ogawa, N. Kosaka, L. T. Rosenblum, P. L. Choyke, H. Kobayashi, *Nat. Med.* **2011**, *17*, 1685–1691; b) X. Li, X.-H. Peng, B.-D. Zheng, J. Tang, Y. Zhao, B.-Y. Zheng, M.-R. Ke, J.-D. Huang, *Chem. Sci.* **2018**, *9*, 2098–2104; c) X. Li, D. Lee, J. D. Huang, J. Yoon, *Angew. Chem. Int. Ed. Engl.* **2018**, *57*, 9885–9890.
[2] P.-C. Lo, M. S. Rodríguez-Morgade, R. K. Pandey, D. K. P. Ng, T. Torres, F. Dumoulin, *Chem. Soc. Rev.* **2020**, *49*, 1041–1056.
[3] B.-D. Zheng, J. Ye, Y.-Y. Huang, M.-T. Xiao, *Biomat. Sci.* **2021**, *9*, 7811–7825.
[4] A. C. S. Lobo, A. D. Silva, V. A. Tomé, S. M. A. Pinto, E. F. F. Silva, M. J. F. Calvete, C. M. F. Gomes, M. M. Pereira, L. G. Arnaut, *J. Med. Chem.* **2016**, *59*, 4688–4696.
[5] B.-D. Zheng, Q.-X. He, X. Li, J. Yoon, J.-D. Huang, *Coord. Chem. Rev.* **2021**, *426*, 213548.
[6] N. Hodgkinson, C. A. Kruger, M. Mokwena, H. Abrahamse, *J. Photochem. Photobiol. B* **2017**, *177*, 32–38.
[7] C. C. Rennie, R. M. Edkins, *Dalton Trans.* **2022**, *51*, 13157–13175.
[8] D. A. Bunin, A. G. Martynov, D. A. Gvozdev, Y. G. Gorbunova, *Biophys. Rev. Lett.* **2023**, *15*, 983–998.
[9] A. W. Snow, in *The Porphyrin Handbook* (Eds.: K. M. Kadish, K. M. Smith, R. Guilard), Academic Press, Amsterdam, **2003**, pp. 129–176.
[10] F. Dumoulin, M. Durmuş, V. Ahsen, T. Nyokong, *Coord. Chem. Rev.* **2010**, *254*, 2792–2847.
[11] a) C. Y. Anderson, K. Freye, K. A. Tubesing, Y. S. Li, M. E. Kenney, H. Mukhtar, C. A. Elmets, *Photochem. Photobiol.* **1998**, *67*, 332–336; b) H. Li, D. E. Marotta, S. Kim, T. M. Busch, E. P. Wileyto, G. Zheng, *J. Biomed. Opt.* **2005**, *10*, 41203.
[12] a) J. Lopes-Nunes, J. Carvalho, J. Figueiredo, C. I. V. Ramos, L. M. O. Lourenço, J. P. C. Tomé, M. G. P. M. S. Neves, J.-L. Mergny, J. A. Queiroz, G. F. Salgado, C. Cruz, *Bioorg. Chem.* **2020**, *100*, 103920; b) A. Gil-Martínez, A. Hernández, C. Galiana-Roselló, S. López-Molina, J. Ortiz, Á. Sastre-Santos, E. García-España, J. González-García, *J. Biol. Inorg. Chem.* **2023**, *28*, 495–507; c) Y. Odahara, A. Momotake, Y. Syokaku, Y. Yamamoto, *ChemBioChem* **2024**, *25*, e202400197.
[13] a) H. Yaku, T. Murashima, D. Miyoshi, N. Sugimoto, *Chem. Commun.* **2010**, *46*, 5740–5742; b) L. Ren, A. Zhang, J. Huang, P. Wang, X. Weng, L. Zhang, F. Liang, Z. Tan, X. Zhou, *ChemBioChem* **2007**, *8*, 775–780; c) L. Zhang, J. Huang, L. Ren, M. Bai, L. Wu, B. Zhai, X. Zhou, *Bioorg. Med. Chem.* **2008**, *16*, 303–312.
[14] K. Kawauchi, W. Sugimoto, T. Yasui, K. Murata, K. Itoh, K. Takagi, T. Tsuruoka, K. Akamatsu, H. Tateishi-Karimata, N. Sugimoto, D. Miyoshi, *Nat. Commun.* **2018**, *9*, 2271.
[15] a) H. Yaku, T. Fujimoto, T. Murashima, D. Miyoshi, N. Sugimoto, *Chem. Commun.* **2012**, *48*, 6203–6216; b) C. I. V. Ramos, S. P. Almeida, L. M. O. Lourenço, P. M. R. Pereira, R. Fernandes, M. A. F. Faustino, J. P. C. Tomé, J. Carvalho, C. Cruz, M. G. P. M. S. Neves, *Molecules* **2019**, *24*, 733; c) J. Lopes-Nunes, J. Carvalho, J. Figueiredo, C. I. V. Ramos, L. M. O. Lourenço, J. P. C. Tomé, M. G. P. M. S. Neves, J.-L. Mergny, J. A. Queiroz, G. F. Salgado, C. Cruz, *Bioorg. Chem.* **2020**, *100*, 103920; d) F. Aydin, E. Bağda, E. Bağda, M. Durmuş, *Polyhedron* **2023**, *238*, 116413.
[16] D. Y. Tam, W. K. M. Lau, Y. T. Limanto, D. K. P. Ng, *ACS Pharmacol. Transl. Sci.* **2024**, *7*, 3216–3227.
[17] J. Kollar, M. Machacek, M. Halaskova, J. Lenco, R. Kucera, J. Demuth, M. Rohlickova, K. Hasonova, M. Miletin, V. Novakova, P. Zimcik, *J. Med. Chem.* **2020**, *63*, 7616–7632.
[18] a) H. Yaku, T. Murashima, D. Miyoshi, N. Sugimoto, *Molecules* **2012**, *17*, 10586–10613; b) M. Uchiyama, A. Momotake, N. Kobayashi, Y. Yamamoto, *Chem. Lett.* **2020**, *49*, 530–533.
[19] K. Kawauchi, W. Sugimoto, T. Yasui, K. Murata, K. Itoh, K. Takagi, T. Tsuruoka, K. Akamatsu, H. Tateishi-Karimata, N. Sugimoto, D. Miyoshi, *Nat. Commun.* **2018**, *9*, 2271.
[20] J. Alzeer, N. W. Luedtke, *Biochemistry* **2010**, *49*, 4339–4348.
[21] a) S. J. Devereux, F. E. Poynton, F. R. Baptista, T. Gunnlaugsson, C. J. Cardin, I. V. Sazanovich, M. Towrie, J. M. Kelly, S. J. Quinn, *Chem. Eur. J.* **2020**, *26*, 17103–17109; b) K. Peterková, M. Stitch, R. Z. Boota, P. A. Scattergood, P. I. P. Elliott, M. Towrie, P. Podbevšek, J. Plavec, S. J. Quinn, *Chem. Eur. J.* **2023**, *29*, e202203250; c) M. Stitch, D. Avagliano, D. Graczyk, I. P. Clark, L. González, M. Towrie, S. J. Quinn, *J. Am. Chem. Soc.* **2023**, *145*, 21344–21360.
[22] K. Oda, S.-i. Ogura, I. Okura, *J. oPhotochem. Photobiol. B:* **2000**, *59*, 20–25.
[23] L. M. Wilhelmsson, F. Westerlund, P. Lincoln, B. Nordén, *J. Am. Chem. Soc.* **2002**, *124*, 12092–12093.
[24] H. Cathcart, V. Nicolosi, J. M. Hughes, W. J. Blau, J. M. Kelly, S. J. Quinn, J. N. Coleman, *J. Am. Chem. Soc.* **2008**, *130*, 12734–12744.
[25] N. Kobayashi, R. Higashi, K. Ishii, K. Hatsusaka, K. Ohta, *Bull. Chem. Soc. Jpn.* **1999**, *72*, 1263–1271.
[26] C. Rennie, E. Sitch, J. Hillis, R. Edkins, *ChemRxiv*. **2022**, DOI: 10.26434/chemrxiv-2022-r25k8.
[27] M. Kasha, H. R. Rawls, M. Ashraf El-Bayoumi, *Pure Appl. Chem.* **1965**, *11*, 371–392.
[28] I. R. Calori, C. C. Jayme, L. T. Ueno, F. B. C. Machado, A. C. Tedesco, *Spectrochim. Acta Part A* **2019**, *214*, 513–521.
[29] S. J. Allen, C. M. Dower, A. X. Liu, K. J. Lumb, *Current Protocols in Chem. Biol.* **2020**, *12*, e78.
[30] E. K. S. McRae, D. E. Nevonen, S. A. McKenna, V. N. Nemykin, *J. Inorg. Biochem.* **2019**, *199*, 110793.
[31] K. N. Luu, A. T. Phan, V. Kuryavyi, L. Lacroix, D. J. Patel, *J. Am. Chem. Soc.* **2006**, *128* (30), 9963–9970.
[32] S. Haider, G. N. Parkinson, S. Neidle, *J. Mol. Biol.* **2002**, *320*, 189–200.
[33] E. N. Ogbonna, A. Paul, A. A. Farahat, J. R. Terrell, E. Mineva, V. Ogbonna, D. W. Boykin, W. D. Wilson, *ACS Bio Med Chem Au* **2023**, *3*, 335–348.
[34] L. Stefan, D. Monchaud, *Nat. Chem. Rev.* **2019**, *3*, 650–668.
[35] Z. A. E. Waller, S. A. Sewitz, S.-T. D. Hsu, S. Balasubramanian, *J. Am. Chem. Soc.* **2009**, *131*, 12628–12633.
[36] a) M. Vorlíčková, I. Kejnovská, J. Sagi, D. Renčiuk, K. Bednářová, J. Motlová, J. Kypr, *Methods* **2012**, *57*, 64–75; b) R. del Villar-Guerra, J. O. Trent, J. B. Chaires, *Angew. Chem. Int. Ed.* **2018**, *57*, 7171–7175.
[37] J. Xia, J. Chen, J. Zhou, M. Cheng, X. Zhuang, C. Cai, H. Ju, J.-L. Mergny, J. Zhou, *J. Phys. Chem. B* **2024**, *128*, 11077–11087.
[38] X. Tu, S. Manohar, A. Jagota, M. Zheng, *Nature* **2009**, *460*, 250–253.
[39] a) M. Zheng, A. Jagota, M. S. Strano, A. P. Santos, P. Barone, S. G. Chou, B. A. Diner, M. S. Dresselhaus, R. S. Mclean, G. B. Onoa, G. G. Samsonidze, E. D. Semke, M. Usrey, D. J. Walls, *Science* **2003**, *302*, 1545–1548; b) R. R. Johnson, A. T. C. Johnson, M. L. Klein, *Nano Letts.* **2008**, *8*, 69–75.
[40] A.-M. Chiorcea-Paquim, A. D. R. Pontinha, A. M. Oliveira-Brett, *Electrochem. Commun.* **2014**, *45*, 71–74.
[41] R. L. Stallings, A. F. Ford, D. Nelson, D. C. Torney, C. E. Hildebrand, R. K. Moyzis, *Genomics* **1991**, *10*, 807–815.

Manuscript received: August 16, 2024
Accepted manuscript online: November 29, 2024
Version of record online: ■■, ■■

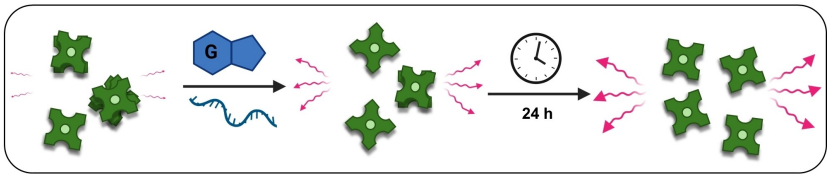

E. R. Windle, Dr. C. C. Rennie, Dr. R. M. Edkins, Prof. S. J. Quinn**

The binding of guanine-rich nucleic acids to a water-soluble cationic, regiopure zinc phthalocyanine (**1**) is reported. In contrast to double-stranded DNA, guanine systems **GpG**, **$(GpG)_{10}$**, **poly(G)** and **quadruplex DNA** effectively disrupt phthalocyanine aggregates to disperse the monomeric state. Time-dependent binding is observed for all systems, especially **poly(G)**. Such biomacromolecule interactions are expected to be important when rationalizing the photoactivity of phthalocyanines in-vivo.